Constructing Detailed Subject-Specific Models of the Human Masseter

C. Antonio Sánchez[1(✉)], Zhi Li[2], Alan G. Hannam[3], Purang Abolmaesumi[1], Anne Agur[2], and Sidney Fels[1]

[1] Department of Electrical and Computer Engineering, University of British Columbia, Vancouver, BC, Canada
antonios@ece.ubc.ca

[2] Department of Surgery, University of Toronto, Toronto, ON, Canada

[3] Faculty of Dentistry, University of British Columbia, Vancouver, BC, Canada

Abstract. We investigate the structural details of the human masseter and their contribution to force-transmission necessary for mastication through a computational modelling study. We compare two subject-specific models, constructed using data acquired by a dissection and digitization procedure on cadaveric specimens. Despite architectural differences between the two masseters, we find that in both instances it is necessary to capture the combination of the multipennate nature of the muscle fibres, as well as the increased aponeurosis stiffness, in order to reproduce adequate clenching forces. We also demonstrate the feasibility of deformably registering these architectural templates to target muscle surfaces in order to create new subject-specific models.

Keywords: Masseter · Mastication · Finite element · Aponeuroses

1 Introduction

Mastication, the chewing of food, is an important process that when hindered can severely affect quality of life. In patients who have undergone treatment for head and neck cancer, muscle damage due to either surgical resection or radiotherapy often leads to reduced comminution efficiency, and can result in chewing or swallowing disorders such as dysphagia. Understanding the mechanics of mastication is crucial if we are to tailor interventions to subjects in order to maximize post-treatment function.

Due to the complexity of the masticatory system, and that functional muscle characteristics are difficult to isolate and measure without interfering with the chewing cycle, computational biomechanical models have become indispensable in studying the process. For simulations to be reliable, however, they must capture all relevant interactions of the coupled system of bones, tendons, muscles, and other soft-tissues, as well as account for any subject-specific variability. To this end, we are developing a detailed model of the masseter, the major muscle involved in mastication, to study the impact of its structural characteristics on function.

M.J. Cardoso et al. (Eds.): BIVPCS/POCUS 2017, LNCS 10549, pp. 52–60, 2017.
DOI: 10.1007/978-3-319-67552-7_7

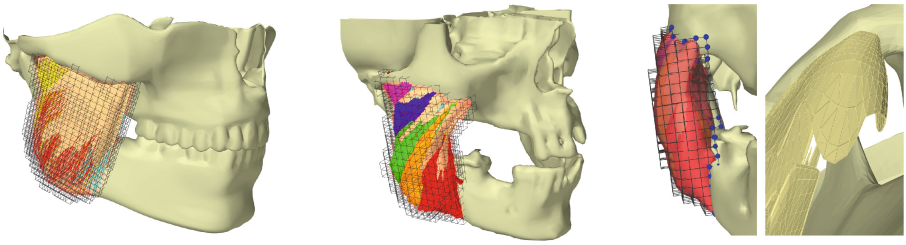

(a) Subject #1 (b) Subject #2 (c) Components

Fig. 1. Finite-element models of the masseter and jaw for simulating clenching force during mastication. The models consist of encapsulating hexahedral muscle volumes, attached to the mandible and zygomatic arch (blue nodes in (c)-left), which are coupled to thin interior membrane-like aponeuroses ((c)-right). (Color figure online)

Most existing models of mastication rely on line-based, lumped-parameter muscle models. Tanaka et al. [15] apply line-based models of the masseter acting on a finite element model (FEM) of the mandible to study stress distributions during teeth clenching. To study the dynamics of jaw-gaping, Hannam et al. [4] developed a complete jaw-hyoid model with line-based muscles. Stavness et al. [14] later used this model to predict muscle activations and forces required for chewing. These line-based representations of the masseter are somewhat limited: they assume muscle uniformity, cannot represent broad attachment areas, and cannot be used to predict stresses within the muscle volume. To examine the impact of surgical intervention or treatment on muscle function, we need a more-detailed three-dimensional representation of the structure.

To our knowledge, Röhrle et al. [12] created the only existing finite-element model of the masseter. They show that using line-based muscles can introduce significant errors in simulated force distributions, to the point where different clinical outcomes could be predicted. One of the limitations of the study was a low prediction of maximum bite force: 77 N, which is quite shy of the potential 200 N+ which has been observed in practice [7]. They note that muscle fibre distribution plays an important role, and suggest that the model can be improved by including a more accurate representation of the muscle architecture.

Unfortunately, the internal details of the masseter are extremely challenging to see using conventional imaging techniques [11]. Because of this, we have acquired two uniquely detailed architectural descriptions of the masseter through dissection and digitization studies. In this work we describe our process for incorporating this data into an efficient hybrid simulation model, which will later be included in a larger complete model for studying mastication.

2 Methods

2.1 Data Collection

Data used for modelling was collected from two human cadaveric studies using the dissection and digitization procedure of Kim et al. [6] (Fig. 2). In this procedure, the formalin embalmed tissue was exposed by removing any skin and superficial fascia. The specimens were securely clamped, and three screws afixed to the bone to act as a frame of reference. The muscle surface was cleaned and delineated to allow each muscle fibre bundle (fascicle) to be traced in its entirety. Digitization of muscle fascicles was carried out using a MicroScribe^{TM} MX Digitizer (0.05 mm accuracy; Immersion Corporation, San Jose, CA). Each fascicle was traced at 3–5 mm intervals between attachment sites. The fibres were then excised to reveal underlying fascicles and aponeuroses. The dissection and digitization process continued until the entire muscle volume was captured. Ethics approval for this study was received from University of Toronto Health Sciences, Mount Sinai Hospital, and University of British Columbia Research Ethics Boards (P.R. #27210, #28530, 12-0252-E, H12-00130).

The first data set, described in Leon et al. [9], was initially collected to study fibre motions during opening and closing of the jaw. Unfortunately, no information regarding aponeuroses was acquired, so for our modelling efforts they were manually drawn based on terminating fibre ends and from anatomical references. For the second specimen, it was decided to additionally digitize the aponeuroses, beginning with the perimeter, then following collagen fibre bundles on the exposed surface. To form three-dimensional sheets of aponeuroses, these outlines were transformed into NURBS curves using Autodesk Maya® and surfaces were lofted between them. A CT scan of the second specimen was also acquired (Aquilion ONE^{TM}, Toshiba Medical Systems Corporation, Tokyo, Japan) with resolution 2 mm × 2 mm and slice thickness of 3 mm. The skull was segmented using thresholding, and manually aligned with the digitized muscle data.

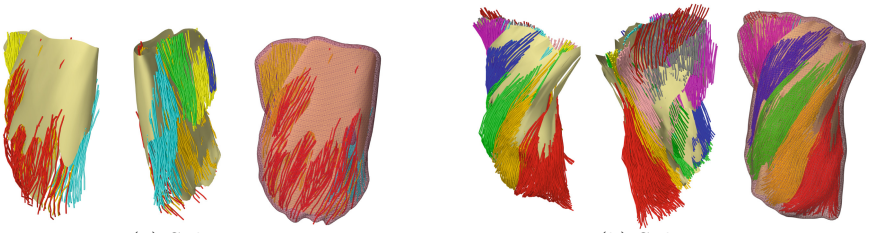

(a) Subject #1 (b) Subject #2

Fig. 2. Digitized muscle fascicles, internal aponeuroses, and encapsulating muscle volume for two subjects. Colours reflect distinct groups of muscle fascicles.

2.2 Finite Element Model Construction

To build volumetric muscle models from the digitized data, we first need to create an encapsulating muscle volume. Similar to Lee et al. [8], we constructed a wrapping surface around the collection of fibres and aponeuroses. For this, we start by computing a three-dimensional distance field on a $100 \times 80 \times 35$ grid of points, determining the distance of each grid point to the nearest 'feature' (either a line-segment from the digitized fibre bundles or face from the triangulated aponeurosis surfaces). We smooth the distance grid by applying the Laplacian smoothing operator, then reconstruct a continuous field by trilinearly interpolating between the grid points. To create the bounding surface, we extract an iso-surface from the smoothed field using the Marching Tetrahedra algorithm [3]. For our masseters, we chose the 2 mm iso-surface.

The next step is to construct the three-dimensional finite-element mesh. Due to the highly incompressible nature of muscle tissue, hexahedral elements are preferred as they avoid common volumetric locking artifacts exhibited by tetrahedral elements. Unfortunately, for our complex geometry including the thin aponeuroses, constructing conforming hexahedral meshes is an extremely challenging and labour-intensive task. Instead, we follow Teran et al. [16], and create a non-conforming bounding finite-element mesh of the entire muscle volume. The result is a voxelized representation, consisting of 1419 and 969 linear 8-node hexahedral elements for the two models (Fig. 1). The muscle-specific material law requires determining the fibre orientation at each point of numerical integration within the FEM volume. We define a fibre field for each compartment of digitized fibre bundles using the method of Sánchez et al. [13]: around each integration point, we examine an influence radius ($r = 2$ mm), and compute a weighted average orientation of all contained digitized fibre segments. These orientations then define the directions of muscle contraction within the corresponding elements.

For the aponeuroses, we extrude the triangulated surface meshes to create 0.5 mm-thin wedge elements. We detach the top nodes of neighbouring elements in order to mimic a membrane, which exhibits in-plane elastic behaviour but zero bending stiffness (Fig. 1c). This allows the aponeuroses to perform their function of transmitting forces to the muscle attachment sites without overly stiffening the entire muscle volume. We then couple the bounding hexahedral FEM and membrane-like aponeurotic sheets using a system of constraints. For each node that falls on the original aponeurosis surface, we compute the values of the FEM interpolation functions $\{\phi_j(\boldsymbol{t})\}$ at rest such that

$$\boldsymbol{t}_i^{(0)} = \sum_j \phi_j\left(\boldsymbol{t}_i^{(0)}\right) \boldsymbol{m}_j^{(0)}, \tag{1}$$

where $\boldsymbol{t}_i^{(0)}$ is the location of the ith node on the aponeurotic sheets at time 0, and $\boldsymbol{m}_j^{(0)}$ is the location of the jth node in the encapsulating muscle volume. To enforce coupling of the models, we maintain this relationship as time progresses, effectively binding the node to its barycentric coordinate within the corresponding muscle element. We can express the constraints as $\mathbf{G}\boldsymbol{n} = 0$, where $\boldsymbol{n}$ is a

concatenated vector of node positions including both muscle nodes $\boldsymbol{m}$ and tendon (aponeurosis) nodes $\boldsymbol{t}$, and $\mathbf{G}$ is a constraint matrix consisting of the fixed interpolation coefficients from Eq. (1).

For our first masseter model (Fig. 1a), we manually aligned the masseter volume with Hannam's existing model for mastication [4] so that fibre bundle ends and aponeuroses aligned with the appropriate origin and insertion sites on the zygomatic arch and angle/ramus of the mandible. For the second model (Fig. 1b), we similarly manually registered the muscle to the skull and jaw extracted from CT. We then attached the muscle volumes to these rigid components by securing nodes to the bones based on proximity as in Fig. 1c.

2.3 Constitutive Laws

We model both the underlying muscle tissue and aponeuroses as incompressible Mooney-Rivlin hyperelastic solids with strain-energy density function

$$W(I_1, I_2, J) = c_1(I_1 - 3) + c_2(I_2 - 3) + \kappa(J - 1)^2, \tag{2}$$

where I_1 and I_2 are the first and second invariants of the Cauchy-Green deformation tensor, and J is the determinant of the deformation gradient. The constants c_1 and c_2 are stiffness parameters, and κ is the bulk modulus responsible for incompressibility. To include the anisotropic contraction behaviour of muscles, we add a material stress based on the Blemker [1] constitutive model:

$$\sigma(\lambda) = \sigma_{\max}\left(\alpha f_{\text{act}}(\lambda) + f_{\text{pass}}(\lambda)\right)(\lambda/\lambda_{\text{opt}}), \tag{3}$$

where $\sigma_{\max}$ is the maximum isometric stress in the muscle, $\alpha \in [0, 1]$ is the normalized muscle activation level, λ is the along-fibre stretch, λ_{opt} is the optimal fibre stretch, and f_{act} and f_{pass} are normalized functions that describe the active and passive force-length relationships for the muscle, respectively (see [1]). For our simulations, we use the same values as Röhrle et al., $c_1 = c_2 = 10$ kPa, $\sigma_{\max} = 300\,\text{kPa}$, and $\lambda_{\text{opt}} = 1.4$. For the aponeurosis material, we increase c_1 and c_2 by a factor of 100 to represent its stiff tensile behaviour.

2.4 Simulation, Registration and Results

For our numerical simulations, we use the open-source ArtiSynth platform [10]. ArtiSynth allows us to combine rigid and deformable elements, along with constraints and coupling, in a hybrid simulation environment. We fix the location of the jaw and skull, activate the muscle, and measure the net isometric contraction force acting between the bones. We take this to be our clenching force contribution from each masseter.

To determine the impact of the various architectural properties, we ran three simulations for each model. In the first, we ignore all internal details, only using the muscle's outer shape with a simplified muscle fibre direction field acting between muscle origin and insertion sites, as in [12]. For the second simulation, we

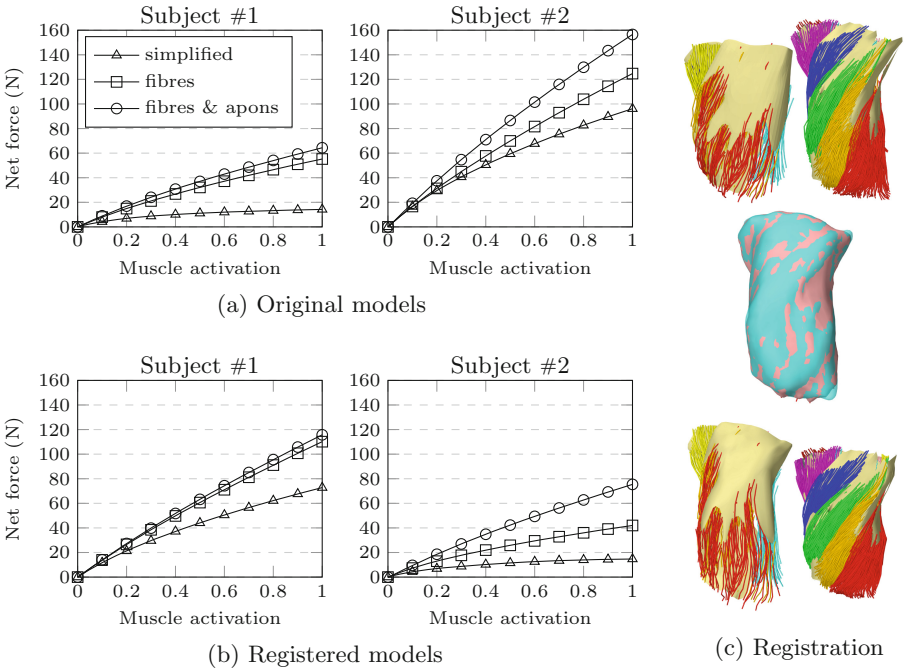

Fig. 3. Force production in the masseter during clenching, applied to both original and registered models. In (c), we see the original (top) and registered (bottom) muscle volumes. The volume from subject #1 (pink) was deformed to fit the muscle surface from subject #2 (cyan). This provides an architectural mapping between the two. (Color figure online)

replace the simplified field with the one derived from muscle fascicle digitization. For the third, we add our thin coupled aponeuroses models, including their stiff tension properties. Force results are shown in Fig. 3a.

In both subject-specific models, use of the simplified directional fibre field resulted in the lowest peak force (14 N, 96 N). Adding the detailed pennated fibre architecture significantly increases force (55 N, 125 N), and incorporating the aponeuroses increased force even further (64 N, 157 N). For subject #1, the aponeuroses did not have as strong an impact as for subject #2. This may be related to our uncertainty in reconstructing the aponeurotic sheets, since the fibre field was less dense and we had no measurements of the collagen fibres. The larger discrepancy between the two models, however, seems to be related to muscle volume. The estimated masseter volume for the first subject, based on the wrapped-fibre surface, is 19.7 cm^3, whereas for the second subject is 38.8 cm^3.

The most reliable predictor of a muscle's peak force is its physiological cross-sectional area (PCSA), which is measured perpendicular to its fibres [8]. The muscle's architecture therefore plays a significant role: the fibre pennation and attachments to internal aponeuroses allow for a larger cross-sectional area within

a fixed volume, resulting in the capacity for stronger contraction forces. For our two models, since the muscle lengths are similar, the doubling of volume is approximately accompanied by a doubling of PCSA, which would in-turn result in a doubling of net force. This is approximately what we seem to be observing.

To remove the impact of muscle volume on our force comparisons, allowing us to better examine the effect of architectural intricacies, we deformably registered the wrapped muscle volumes together (Fig. 3c). We use the FEM-based deformable registration technique of Khallaghi et al. [5] with parameters: $\beta = 1000$, $E = 60$ kPa, $\nu = 0.49$, $w = 0.05$. This technique accounts for changes in scale, estimates soft-correspondences between points on the two surfaces, and attempts to minimize strain energy while deforming one dataset to the other. The deformation map is invertible, allowing us to construct two new registered models: one in the space of subject #1, and one in the space of subject #2. We re-ran the clenching simulations, and report results in Fig. 3b. Again, we notice similar influence of the fibre field and aponeuroses, and that force seems to be approximately scaled with muscle volume as expected.

3 Conclusions

In this work, we examined the impact of modelling a detailed fibre and aponeurosis architecture on force transmission in the masseter for two subjects. We showed that by including both the pennated fibre field and the stiff aponeurotic sheets, we were able to increase simulated maximum bite forces to more realistic levels in subject #2 (167 N *vs.* 96 N). In subject #1, we also saw gains in force, but the values themselves were much smaller. We hypothesize that we are currently under-representing the muscle volume for this subject, which seems to be confirmed by registering the model to the muscle volume of subject #2. This resulted in an increased maximum net force from 64 N to 157 N.

The dissection process clearly cannot be used to extract architectural details in live subjects. Instead, we propose to register our current digitized templates to muscle surfaces extracted by other means such as image segmentation. We demonstrated the feasibility of this approach by registering our two masseters together to create two new registered models. The force patterns in the registered models are on similar orders of magnitude as their target counterparts, but still do exhibit differences. This suggests that a significant portion of force-production can be accounted-for by adjusting for muscle shape and volume, but that subject-specific architectural variability may still play an important role. With new advanced imaging techniques (e.g. [2]), we may be able to obtain some of these internal muscle details *in vivo*. We could then combine this data with our template-based approach, using it for both for template selection and for adding internal targets during registration. Such a hybrid technique would allow us to quickly and efficiently generate subject-specific models of the masseter for studying and analyzing the functional impact of treatment on mastication.

Acknowledgments. This work was supported by the Natural Sciences and Engineering Research Council of Canada (NSERC), the Canadian Institutes of Health Research (CIHR), and the University of British Columbia.

References

1. Blemker, S., Pinsky, P., Delp, S.: A 3D model of muscle reveals the causes of nonuniform strains in the biceps brachii. J. Biomech. **38**(4), 657–665 (2005)
2. Cioffi, I., Gallo, L.M., Palla, S., Erni, S., Farella, M.: Macroscopic analysis of human masseter compartments assessed by magnetic resonance imaging. Cells Tissues Organs **195**(5), 465–472 (2012)
3. Doi, A., Koide, A.: An efficient method of triangulating equi-valued surfaces by using tetrahedral cells. IEICE Trans. Inf. Syst. **74**(1), 214–224 (1991)
4. Hannam, A., Stavness, I., Lloyd, J., Fels, S.: A dynamic model of jaw and hyoid biomechanics during chewing. J. Biomech. **41**(5), 1069–1076 (2008)
5. Khallaghi, S., Sánchez, C.A., Rasoulian, A., Nouranian, S., Romagnoli, C., Abdi, H., Chang, S.D., Black, P.C., Goldenberg, L., Morris, W.J., Spadinger, I., Fenster, A., Ward, A., Fels, S., Abolmaesumi, P.: Statistical biomechanical surface registration: application to MR-TRUS fusion for prostate interventions. IEEE Trans. Med. Imaging **34**(12), 2535–2549 (2015)
6. Kim, S.Y., Boynton, E.L., Ravichandiran, K., Fung, L.Y., Bleakney, R., Agur, A.M.: Three-dimensional study of the musculotendinous architecture of supraspinatus and its functional correlations. Clin. Anat. **20**(6), 648–655 (2007)
7. Koolstra, J., van Eijden, T., Weijs, W., Naeije, M.: A three-dimensional mathematical model of the human masticatory system predicting maximum possible bite forces. J. Biomech. **21**(7), 563–576 (1988)
8. Lee, D., Ravichandiran, K., Jackson, K., Fiume, E., Agur, A.: Robust estimation of physiological cross-sectional area and geometric reconstruction for human skeletal muscle. J. Biomech. **45**(8), 1507–1513 (2012)
9. Leon, L.M., Liebgott, B., Agur, A.M., Norwich, K.H.: Computational model of the movement of the human muscles of mastication during opening and closing of the jaw. CMBBE **9**(6), 387–398 (2006)
10. Lloyd, J.E., Stavness, I., Fels, S.: ArtiSynth: a fast interactive biomechanical modeling toolkit combining multibody and finite element simulation. In: Payan, Y. (ed.) Soft Tissue Biomechanical Modeling for Computer Assisted Surgery. Studies in Mechanobiology, Tissue Engineering and Biomaterials, vol. 11, pp. 355–394. Springer, Heidelberg (2012). doi:10.1007/8415_2012_126
11. Raadsheer, M., van Eijden, T., van Spronsen, P., van Ginkel, F., Kiliaridis, S., Prahl-Andersen, B.: A comparison of human masseter muscle thickness measured by ultrasonography and magnetic resonance imaging. Arch. Oral Biol. **39**(12), 1079–1084 (1994)
12. Röhrle, O., Pullan, A.J.: Three-dimensional finite element modelling of muscle forces during mastication. J. Biomech. **40**(15), 3363–3372 (2007)
13. Sánchez, C.A., Lloyd, J.E., Fels, S., Abolmaesumi, P.: Embedding digitized fibre fields in finite element models of muscles. Comput. Methods Biomech. Biomed. Eng. Imaging Vis. **1**(4) (2013)
14. Stavness, I., Hannam, A.G., Lloyd, J.E., Fels, S.: Predicting muscle patterns for hemimandibulectomy models. CMBBE **13**(4), 483–491 (2010)

15. Tanaka, E., Tanne, K., Sakuda, M.: A three-dimensional finite element model of the mandible including the tmj and its application to stress analysis in the tmj during clenching. Med. Eng. Phys. **16**(4), 316–322 (1994)
16. Teran, J., Sifakis, E., Blemker, S., Ng-Thow-Hing, V., Lau, C., Fedkiw, R.: Creating and simulating skeletal muscle from the visible human data set. IEEE Trans. Vis. Comput. Graph. **11**(3), 317–328 (2005)